Clays and Clay Minerals, Vol. 54, No. 3, 351–362, 2006.

CLAY MINERALS IN EARLY AMPHIBOLE WEATHERING: TRI- TO DIOCTAHEDRAL SEQUENCE AS A FUNCTION OF CRYSTALLIZATION SITES IN THE AMPHIBOLE

D. PROUST[1],*, J. CAILLAUD[2] AND C. FONTAINE[1]

[1] UMR 6532 CNRS, HydrASA, Faculté des Sciences, 40 Avenue du recteur Pineau, 86022 Poitiers cedex, France
[2] UMR 8013 CNRS, ELICO, Université du Littoral Côte d'Opale, MREN, 32 Avenue Foch, 62930 Wimereux, France

Abstract—The early stages of amphibole weathering result in the crystallization of several clay mineral species: tri- and dioctahedral smectites, interstratified dioctahedral kaolinite-smectite (K-S), and halloysite. Each clay mineral crystallizes into specific microsites which develop from etch pits along specific crystallographic directions in the host amphibole. Two types of microsites are recognized according to their location in the amphibole crystal and their clay mineral crystallizations. The first type is a plane surface related to the (110) amphibole cleavages where saponite particles crystallize in a characteristic honeycomb texture. The second type is a 'sawtooth' (001) fracture surface generated by etch-pit coalescence where (1) platy K-S particles crystallize directly in contact with the amphibole at the top of 'teeth', (2) halloysite particles with tubular habits crystallize directly in contact with the amphibole on the side of the 'teeth', and/or on the K-S particles, and (3) montmorillonite crystallizes in the central part of the (001) fracture as a layer with honeycomb texture in contact with the K-S platelets located at the top of 'teeth'. The microtextural relationships between the clay minerals and their host mineral suggest the following crystallization sequence: (1) saponite and montmorillonite crystallize first on the (110) and (001) surfaces, respectively; (2) as amphibole dissolution proceeds perpendicular to the (001) fracture planes, montmorillonites continue to form in the middle part of the widening fracture whereas K-S crystallizes on the 'sawtooth' termination; (3) in the last stage of weathering, tubular halloysite crystallizes on the side of the 'teeth', and/or on the K-S.

Key Words—Amphibole, Halloysite, Kaolinite-smectite Mixed-layers, Montmorillonite, Saponite, Weathering.

INTRODUCTION

The weathering of ferromagnesian silicate minerals has been studied extensively over the last three decades, either under experimental conditions (Luce *et al.*, 1972; Schott *et al.*, 1981; Wegner and Christie, 1985; Brantley and Chen, 1995; Zhang *et al.*, 1996; Zhang and Bloom, 1999a, 1999b), or in natural environments (Wilson and Farmer, 1970; Cole and Lancucki, 1976; Eggleton, 1982; Proust, 1982, 1985; Velbel, 1989; Abreu and Vairinho, 1990; Banfield and Barker, 1994; Dreher and Niederbudde, 2000; Bain *et al.*, 2001). These studies demonstrated that pyroxenes and amphiboles are highly reactive minerals under weathering conditions and act as the main potential feeders of Mg and Fe for clay mineral formation in saprolites and soils. Two crystallization processes are currently invoked for clay mineral formation in pyroxenes and amphiboles, depending on the solid/fluid ratio in the natural weathering systems: (1) solid-state transformations in the early stages of weathering with high solid/fluid ratio produce clay minerals in specific topotactic relations with the parent structures. Pyroxene and amphibole habits are preserved and their weathering products retain most of their chemical and structural characteristics (Eggleton and Smith, 1983; Baronnet, 1997). As a consequence, Fe- and Mg-rich 2:1 layer-type clay minerals such as talc, saponite, nontronite, vermiculite and Fe-montmorillonite may form (Eggleton, 1975, 1982; Cole and Lancucki, 1976; Ildefonse *et al.*, 1979; Abreu and Vairinho, 1990; Banfield and Barker, 1994). (2) Dissolution/crystallization mechanisms dominate in more advanced weathering stages with low solid/fluid ratio. Pyroxene and amphibole habits are no longer preserved and the crystallochemistry of their weathering products is now mainly controlled by the solutions, with intense leaching of the most mobile elements (Ca, Mg and Na) and trapping of Fe (Fe^{3+} oxidation state) into oxides and hydroxides. Thus, newly-formed clay minerals gain Al as weathering systems open to meteoric solutions, giving way to the well-known weathering sequences at the scale of the saprolites: dioctahedral 2:1 to 1:1 layer-type clay minerals, with intermediate mixed-layered structures (Wilson, 1987; Righi *et al.*, 1998, 1999; Velbel, 1989; Kampf *et al.*, 1995; Dreher and Niederbudde, 2000; Islam *et al.*, 2002).

Petrographic studies of weathered rocks showed that saprolites were made up of successive weathered levels with preserved or obliterated initial rock texture.

* E-mail address of corresponding author:
dominique.proust@hydrasa.univ-poitiers.fr
DOI: 10.1346/CCMN.2006.0540306

Moreover, each level contained specific chemical micro-environments and clay minerals, the nature of the latter depending on the degree of micro-environments opening to solutions (Proust and Velde, 1978; Ildefonse, 1980; Proust, 1982, 1985; Righi and Meunier, 1995; Caillaud *et al.*, 2004). However, these studies were conducted at the scale of the chemical weathering microsystems, *i.e.* the 50−10 μm scale and did not allow direct observation of the weathering mineral/crystallizing clay mineral interface. The current project was thus designed to improve our insight into textural and crystallochemical relationships between parent mineral and weathering products at crystal scale, *i.e.* infra-micrometer, and to determine whether similar chemical microsystems may coexist in a single amphibole grain in its initial weathering stage.

MATERIALS AND METHODS

Materials

The amphibolite investigated is part of one of the peridotite-serpentinite-amphibolite associated complexes which form numerous roughly lenticular bodies in Limousin. The study site is located in Haute-Vienne (Limousin, France), 30 km south of Limoges, near the Puycheny village (N45º36′27″; E1º09′45″). The amphibolite saprolite was selected in the deepest part of a tile factory quarry where unweathered rock is exposed at 6 m depth (Figure 1).

Fresh rock is dark-green with white feldspars denoting a foliation. The foliation surfaces ('S' fabric) are 2 cm apart and strike 74ºN with a slight dip ranging from 22º to 28ºSE. The thin-sections show the grain size to vary between 0.2 and 1.0 mm with a mineralogy including amphiboles 70%, plagioclases 25%, quartz and accessory Fe oxides 5%. The good alignment of amphibole and plagioclase grains gives a regular lineation ('L' fabric) to the rock. Three weathering zones were recognized as a function of the degree of alteration of the primary rock fabric. The amphibolite begins to weather between 5.80 and 3.80 m into a pale-brown coherent saprolite level (Sap 1, Figure 1) where initial rock fabric is still preserved. The amphibole lineation retains its original dark-green color and texture whereas weathered plagioclases acquire a chalky friable aspect with widened lineation. Pervasive rock weathering is observed between 3.80 and 1.50 m as a gray whitish level (Sap 2, Figure 1) which is marked by the progressive replacement of the original rock fabric by a clayey plasma. The plagioclases disappear completely whereas yellowish-brown remnants of the amphibole lineation are still observed at the top of this level, embedded into a white plasma produced by the weathering of plagioclases. The top of the saprolite, from 1.50 m to surface (Sap 3, Figure 1), is marked by a complete modification of the fabric which coincides with the disappearance of the amphibole lineation. The rock structure is totally obliterated by the large development of a yellowish-brown clayey plasma with Fe oxides and hydroxides as red-brown patches disseminated into the clayey material or lining subvertical fissures.

Methods

Each sample was collected carefully as an undisturbed block to preserve the original fabric of the rock and its weathered facies. Each block was further divided in two parts. The first part of the sample, devoted to the

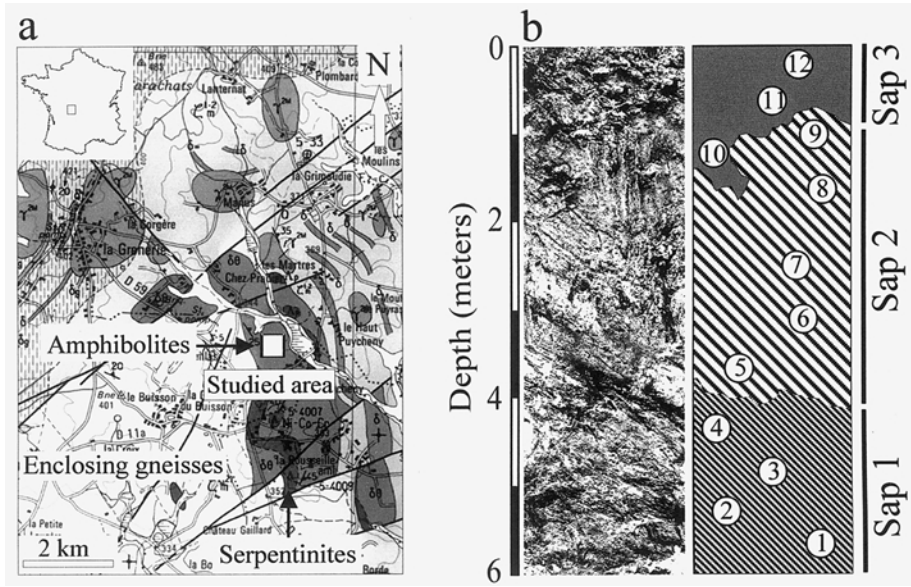

Figure 1. Location and sketch of the amphibolite weathering profile: (a) geological setting; (b) structures of horizons Sap 1, Sap 2, Sap 3 and sampling locations (from 1 to 12).

amphibole crystal separation, was disaggregated by gentle shaking in water, and sieved. The amphibole grains were separated from the sandy fractions (80–100 μm, 100–150 μm, 150–250 μm and 250–500 μm) using bromoform heavy liquid (specific gravity 2.89 g cm^{-3}). Separation efficiency was checked by X-ray diffraction (XRD); the amphibole grains were affixed to glass plates with double-sided adhesive tape and carbon coated for scanning electron microscopy (SEM) study. A JEOL JSM 5600-LV microscope was used with an OXFORD energy dispersive X-ray spectrometer for scanning electron micro-analyses (SEMA) of the amphibole grains and their weathering products. The clay minerals observed and analyzed under SEM were extracted from the amphibole grains by ultrasonic treatment and separated into <0.2 μm and 0.2 μm–2 μm fractions by centrifugation of the supernatant liquid. These clay minerals were then identified by XRD on random powders and Ca-saturated oriented preparations using a PHILIPS PW 1730 diffractometer (40 kV, 40 mA) with Ni-filtered CuKα radiation. The XRD patterns were recorded using a stepping motor-driven goniometer with a DACO-MP recorder using the Diffrac AT software (Socabim). The XRD patterns were then decomposed into their elementary curves using the DecompXR decomposition program (Lanson, 1993). The Newmod program by Reynolds (1985) was used to simulate XRD patterns and to identify and quantify the mixed-layered clay minerals.

The second part of the sample, devoted to electron microprobe analyses (EMPA), was impregnated with epoxy resin to achieve diamond-polished thin-sections with the original sample fabric preserved. The weathering microsites of the amphiboles were first located on the thin-sections and then analyzed *in situ* using a CAMECA SX 50 electron microprobe (WDS analysis) at the 'Service d'analyse CAMPARIS', University of Paris VI. The analytical conditions were as follows: accelerating voltage of 15 kV, beam size of 1 μm, beam current of 4 nA, counting time of 10 s for each analyzed element.

As the EMPA and SEMA data were consistent (closed mean and standard deviation), the results of the analyses were combined in Tables 1 and 2 and plotted in the M^{+}-4Si-R^{2+} chemiographic representation which distributes the major dioctahedral and trioctahedral

Table 1. Chemical composition (wt.%) of the amphiboles from sample 1.

	Magnesio-hornblende		Actinolite		Actinolitic hornblende		Tschermakitic hornblende	
	Mean, n = 49*	σ	Mean, n = 14	σ	Mean, n = 19	σ	Mean, n = 5	σ
SiO_2	47.06	1.33	54.39	1.25	50.86	0.52	44.90	0.55
TiO_2	0.59	0.16	0.08	0.06	0.22	0.07	0.69	0.06
Al_2O_3	11.66	2.48	3.93	1.16	5.54	0.40	14.13	0.37
Cr_2O_3	0.10	0.12	0.21	0.49	0.06	0.06	0.32	0.42
Fe_2O_3**	3.85	1.75	0.00	1.01	2.83	1.46	5.27	0.24
FeO**	8.17	1.48	6.90	2.22	7.16	1.31	8.32	0.41
MnO	0.22	0.12	0.16	0.10	0.24	0.13	0.30	0.20
MgO	12.67	1.61	16.88	0.65	15.92	0.40	11.30	0.29
CaO	11.41	0.93	13.29	3.11	12.13	0.30	11.31	0.36
Na_2O	1.04	0.18	0.40	0.38	0.53	0.12	1.35	0.09
K_2O	0.28	0.10	0.04	0.05	0.12	0.06	0.35	0.04
Total	97.06		96.29		95.59		98.25	
Structural formulae calculated on the basis of 23 oxygens								
Si	6.79		7.73		7.38		6.46	
^{IV}Al	1.21		0.27		0.62		1.54	
^{VI}Al	0.77		0.39		0.32		0.86	
Ti	0.06		0.01		0.02		0.07	
Cr	0.01		0.02		0.01		0.04	
Fe^{3+}	0.43		0.00		0.31		0.57	
Fe^{2+}	0.97		0.82		0.87		1.00	
Mn	0.03		0.02		0.03		0.04	
Mg	2.72		3.58		3.44		2.42	
Ca	1.76		2.02		1.88		1.74	
Na	0.29		0.11		0.15		0.38	
K	0.05		0.01		0.02		0.06	
(Ca+Na) (B)	2.00		2.02		2.00		2.00	
Na (B)	0.24		0.00		0.12		0.26	
(Na+K) (A)	0.11		0.12		0.05		0.18	
$Mg/(Mg+Fe^{2+})$	0.74		0.81		0.80		0.71	

* n = number of analyses; **Fe_2O_3 and FeO contents calculated according to Mössbauer data.

Table 2. Chemical composition (wt.%) of smectites, K-S and halloysite in amphiboles from sample 1.

	Saponite Mean n = 17*	σ	Montmorillonite Mean n = 18	σ	K-S 1 Mean n = 13	σ	K-S 2 Mean n = 14	σ	Halloysite Mean n = 11	σ
SiO_2	46.89	3.53	50.50	4.62	47.04	3.68	43.53	1.67	44.78	0.95
TiO_2	0.20	0.11	0.08	0.10	0.05	0.07	0.03	0.04	0.04	0.04
Al_2O_3	13.69	1.97	19.04	4.19	25.86	3.40	31.26	1.86	32.61	0.76
Cr_2O_3	0.02	0.08	0.01	0.03	0.02	0.04	0.04	0.05	0.05	0.05
Fe_2O_3**			8.18	2.91	5.72	2.49	6.60	0.94	5.99	0.42
FeO**	11.89	1.79	13.47	1.97						
MnO	0.05	0.08	0.04	0.05	0.02	0.05	0.03	0.05	0.04	0.05
MgO	9.94	4.51	2.50	0.44	1.48	0.39	0.20	0.19	0.09	0.03
CaO	1.41	0.56	1.61	0.34	1.06	0.25	0.19	0.19	0.09	0.05
Na_2O	0.32	0.40	0.14	0.16	0.14	0.12	0.13	0.05	0.14	0.04
K_2O	0.38	0.29	0.37	0.29	0.23	0.20	0.12	0.09	0.12	0.05
Total	84.79		82.47		81.62		82.13		83.94	
Structural formulae calculated on the basis of 11 oxygens									7 oxygens	
Si	3.55		3.71		3.45		3.18		2.03	
^{IV}Al	0.45		0.29		0.55		0.82		0.00	
Σtet.	4.00		4.00		4.00		4.00		2.03	
^{VI}Al	0.77		1.36		1.69		1.87		1.74	
Ti	0.01		0.00		0.00		0.00		0.00	
Cr	0.00		0.00		0.00		0.00		0.00	
Fe^{3+}			0.45		0.32		0.36		0.20	
Fe^{2+}	0.75									
Mn	0.00		0.00		0.00		0.00		0.00	
Mg	1.12		0.27		0.16		0.02		0.01	
Σoct.	2.65		2.08		2.17		2.25		1.95	
Ca	0.11		0.13		0.08		0.01		0.00	
Na	0.05		0.02		0.02		0.02		0.01	
K	0.04		0.03		0.02		0.01		0.02	
Int. ch.	0.31		0.31		0.20		0.05		0.03	

* n = number of analyses; **total iron expressed as FeO in saponite and Fe_2O_3 in montmorillonite; σ = standard deviation Σtet. = total tetrahedral occupation; Σoct. = total octahedral occupation; Int. ch. = interlayer charge.

clay minerals into well-separated chemical domains. The chemiographic poles were calculated as:

$$M^{+} = 2Ca^{2+} + Na^{+} + K^{+},\ 4Si = Si^{4+}/4 \text{ and}$$
$$R^{2+} = Fe^{2+} + Mg^{2+} + Mn^{2+}.$$

RESULTS

Mineralogy and SEM morphology of amphiboles

The macroscopic examination of the separated amphiboles shows that most grains fall in the 200−500 µm size range and occur as dark green euhedral prismatic crystals with (001) planes showing the characteristic two cleavage planes. The early weathering patterns of amphiboles appear in grains extracted at 5.80 m depth, at the bottom of the saprolite (sample 1, Figure 1) where cleavage planes widen and are underlined by whitish clayey infillings.

The XRD random powder patterns of the amphiboles extracted from sample 1 are similar for all size fractions with two strong (110 and 310) reflections at 8.340 Å and 3.120 Å characteristic of the calcic amphibole group (Figure 2a). The decomposition of the XRD pattern of the 250−500 µm amphibole fraction in the 020−110 and 240−310 angular ranges (Figure 2b) characterizes a mixture of dominant magnesio-hornblende [020−110 doublet at 9.030 Å and 8.420 Å, 240−310 doublet at 3.276 Å and 3.126 Å] with actinolite [020−110 doublet at 9.100 Å and 8.510 Å, 240−310 doublet at 3.284 Å and 3.135 Å].

Microscopic examination of thin-sections from sample 1 (Figure 3a) shows euhedral prismatic crystals cut in various orientations: (1) crystals cut perpendicular to the z axis exhibit two cleavage traces at characteristic amphibole angles (~60:120°); (2) crystals cut parallel to the z axis show the excellent prismatic cleavage on (110) with slightly inclined (<30°) extinction, high relief and pale yellow to green pleochroism under plane-polarized light.

The chemical data (Table 1) reveal that the amphiboles belong to the calcic group with $(Ca + Na)_B \geqslant 1.34$ and $Na_B < 0.67$ according to the IMA nomenclature (1978). Their ferric Fe content was determined to be 32% of total Fe using Mössbauer spectroscopy; their $Mg/(Mg + Fe^{2+})$ ratio ranges from 0.55 to 0.85, from Tschermakitic hornblende to actinolite with dominant

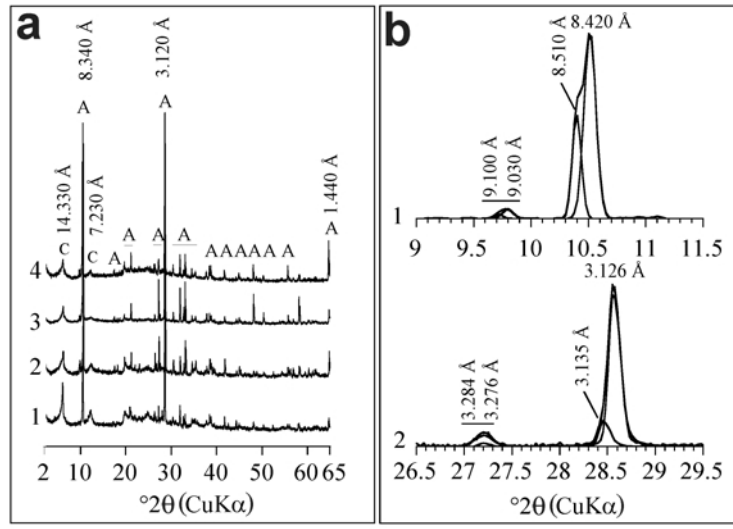

Figure 2. XRD patterns of the amphiboles separated from sample 1. (a) Random powders of fractions 80−100 μm (1), 100−150 μm (2), 150−250 μm (3) and 250−500 μm (4); A = amphibole, C = clay mineral; (b) decomposition of the XRD pattern of the 250−500 μm amphibole fraction in the 020−110 and 240−310 angular ranges (1 and 2).

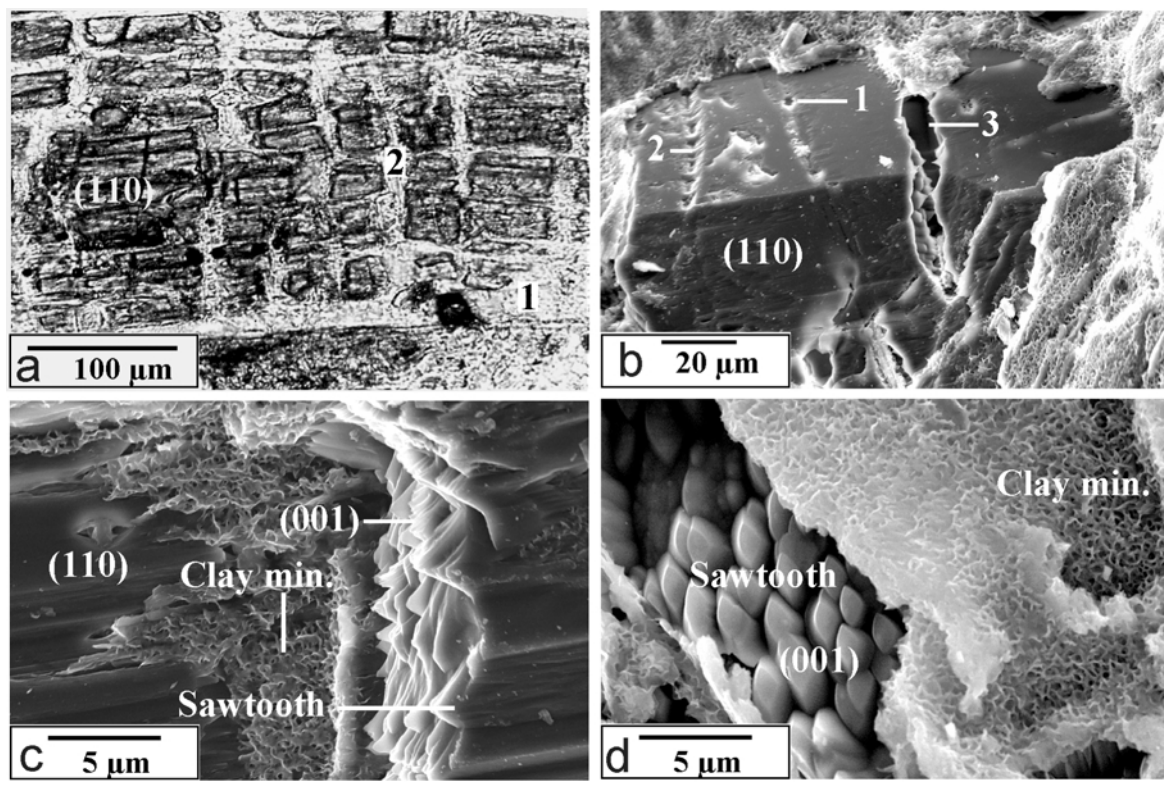

Figure 3. Microscope and SEM observations of the first weathering features and clay mineral locations in amphibole grains from sample 1. (a) (110) amphibole section under plane-polarized light; (1) intramineral microcracks from widening amphibole cleavage planes; (2) transverse microcracks intersecting the amphibole cleavages. (b) SEM view of the (110) faces from a corroded amphibole grain: (1) almond-shaped etch pit; (2) coalescence of almond-shaped etch pits; (3) opening of a (001) microcrack. (c) SEM view of (001) microcrack with sawtooth termination and honeycomb clay mineral crystallization upon a (110) amphibole surface (Clay min.). (d) SEM view of a (001) microcrack with sawtooth termination and honeycomb clay mineral crystallization upon a (001) denticulated amphibole surface (Clay min.).

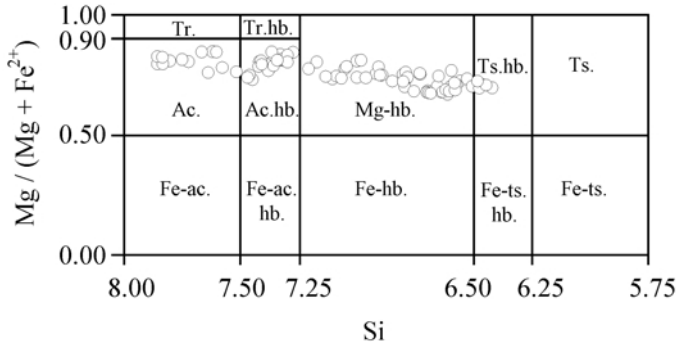

Figure 4. Chemical compositions of the unweathered amphiboles (sample 1) as they plot in the clasification diagram of the calcic amphiboles derived from IMA (1978).

magnesio-hornblende chemistry in terms of their Si ⇌ ^{IV}Al substitutions (Figure 4).

The first weathering features of amphibole develop from intramineral microcracks, 1−10 μm wide, with two specific orientations within the amphibole crystal (Figure 3a): (1) widening of (110) amphibole cleavages produces intramineral microcracks where clay minerals with second-order yellow polarization colours crystallize; (2) transverse microcracks intersect the amphibole (110) cleavages and are filled with first-order gray clay minerals. The SEM study reveals that amphibole dissolution begins on (110) surfaces with the formation of almond-shaped etch pits aligned parallel to the amphibole *c* axis (Figure 3b). These etch pits coalesce to produce micrometric cracks perpendicular to the (110) surface with sawtooth amphibole terminations in the (001) plane (Figure 3c). The (110) and denticulated (001) planes are covered by clay minerals with characteristic honeycomb texture (Figure 3c,d).

Mineralogy and SEM morphology of weathering products

The clay minerals extracted from the amphibole grains after ultrasonic treatment are mineralogically different according to the granulometric fraction studied (<0.2 μm and 0.2−2 μm). The XRD patterns of the Ca-saturated 0.2−2 μm clay fraction (Figure 5a) exhibit diffraction bands typical of smectite: strong reflection at 15.170 Å with weak higher orders at 7.500, 3.700 and 3.040 Å in the air-dried state, 17.580 Å reflection with

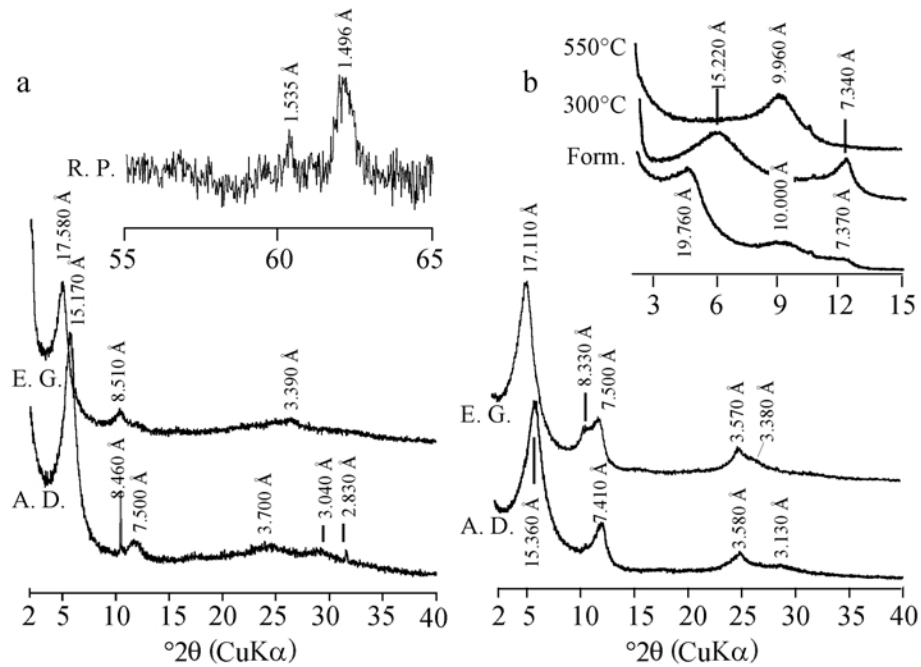

Figure 5. XRD patterns of clay minerals extracted from the amphibole grains (sample 1): (a) Ca-saturated 0.2−2 μm clay fraction; (b) Ca-saturated <0.2 μm clay fraction. A.D. = air-dried state; E.G. = ethylene glycol solvated; R.P. = random powder; Form. = formamide treated; 300ºC and 550ºC heated.

higher orders at 8.510 and 3.390 Å after ethylene glycol solvation. Additional reflections at 8.460 and 2.830 Å are attributed to amphibole remnants. The 060 reflections at 1.535 and 1.496 Å on random powders characterize two types of smectitic minerals, trioctahedral and dioctahedral, respectively. The XRD patterns of the Ca-saturated <0.2 μm clay fraction (Figure 5b) show the characteristics of a more complex assemblage: (1) a smectite typified by a strong reflection at 15.360 Å with higher orders at 7.410, 3.580 and 3.130 Å in the air-dried state, 17.110−3.380 Å reflections after ethylene glycol solvation, 19.760 Å after formamide treatment, and 9.960 Å after heating at 550ºC; (2) a halloysite typified by reflections at 7.410 Å (superimposed on a 002 smectite reflection) and 3.580 Å in the air-dried state, 7.500 Å and 3.570 Å reflections after ethylene glycol solvation, swelling at 10.000 Å after formamide treatment, and disappearing after heating at 550ºC. However, the XRD pattern for the ethylene glycol-solvated sample does not exhibit the characteristic well-resolved 8.510 Å 002 reflection of expanded smectite, but rather a large 'saddle' between 8.330 Å and 7.500 Å, also observed between 3.570 Å and 3.380 Å. This 'saddle' effect is characteristic of mixed-layer kaolinite-smectite (K-S), as described by Righi *et al*. (1999).

The XRD pattern of the Ca-saturated, ethylene glycol-solvated, <0.2 μm clay fraction has been decomposed in the 7−15º2θ and 20−30º2θ regions, respectively (Figure 6). Five main derived curves are obtained in the 7−15º2θ region with maxima at 8.540, 8.420, 8.140, 7.490 and 7.390 Å (Figure 6a). In the 20−30º2θ region, four main curves are obtained with maxima at 3.580, 3.520, 3.440 and 3.360 Å (Figure 6b).

The 8.420 Å peak is attributed to amphibole remnants whereas the peaks at 8.540 and 3.360 Å are attributed to expanded smectite layers. The 8.140 and 3.440 Å peaks characterize R = 0 K-S with 60% kaolinite layers (K-S 1)

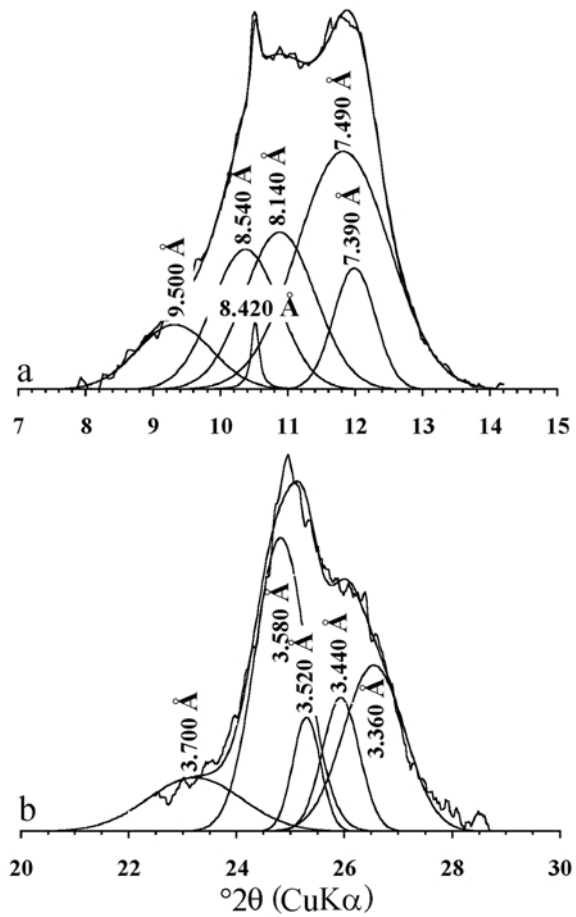

Figure 6. Decomposition of the Ca-saturated, ethylene glycol-solvated XRD pattern of the <0.2 μm clay fraction extracted from the amphibole grains (sample 1).

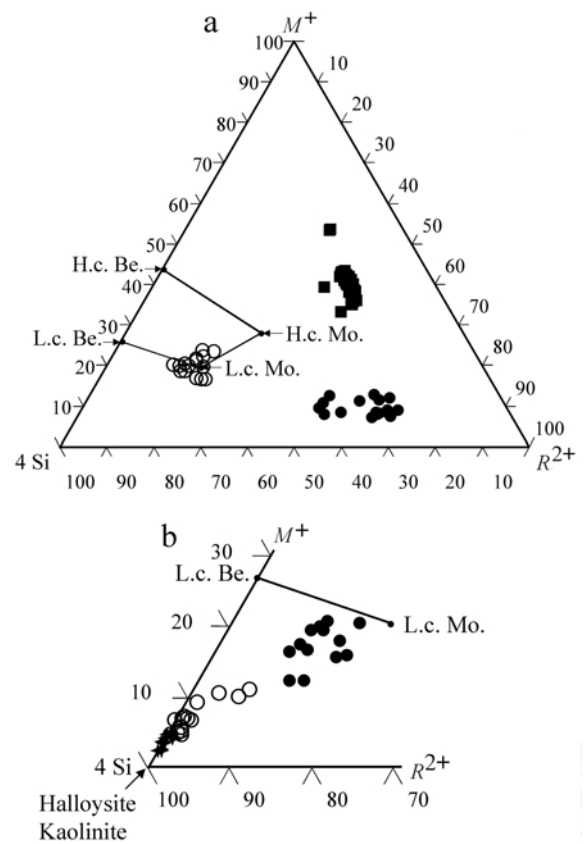

Figure 7. Chemical compositions of amphiboles and their associated clay minerals as they plot in the M^{+}-4Si-R^{2+} ternary diagram. Thick lines delimit the chemical domains of dioctahedral smectites with low-charge beidellite (L.c. Be.), high-charge beidellite (H.c. Be.), low-charge montmorillonite (L.c. Mo.) and high-charge montmorillonite (H.c. Mo.) end-members. (a) Black squares = amphiboles; black circles = saponites; open circles = montmorillonites. (b) Enlarged view of the chemical domain between low-charge dioctahedral smectites and halloysite; black circles = mixed-layer K-S 1; open circles = mixed-layer K-S 2; crosses = halloysite.

whereas 7.390 and 3.520 Å peaks typify R = 0 K-S with 86% kaolinite layers (K-S 2), as obtained using Newmod XRD simulations. The most intense peaks at 7.490 and 3.580 Å are attributed to the halloysite component. Additional large reflections at 9.500 and 3.700 Å are attributed to shoulders of the 8.140 and 3.440 Å peaks which appear in Newmod when simulating R=0 K-S with 60% kaolinite layers and a small coherent diffraction domain (low N = 3, high N = 7).

The chemical compositions of these clay minerals are given in Table 2 and plotted in the M^{+}-4Si-R^{2+} ternary diagram in Figure 7.

Two chemically distinct smectite populations occur (Table 2, Figure 7a) with specific crystallization sites in the amphibole grains (Figure 8). The first population is observed on the (110) amphibole cleavage surfaces as clay particles organized in honeycomb texture (Figure 8a); it is composed of low-charged trioctahedral smectites (mean interlayer charge of 0.31 and mean octahedral occupancy of 2.65 per half unit-cell) with Mg-Fe rich saponite compositions (1.12 Mg atoms and 0.75 Fe atom per half unit-cell). The second population is observed covering the (001) amphibole denticulated fractures with honeycomb (Figure 8a,b) or spherulitic (Figure 8c,d) textures; it is composed of low-charged dioctahedral smectites (mean interlayer charge of 0.31 and mean octahedral occupancy of 2.08 per half unit-cell) with aluminous montmorillonite compositions (1.65 total Al atoms per half unit-cell).

An SEM study of more advanced weathering stages reveals that the (001) amphibole denticulated fractures are covered with platy clay minerals whereas tubular ones can form directly in contact with the amphibole tooth or on the platy clay minerals (Figures 9, 10). The chemistry of these minerals (Table 2) reveals that platy particles plot into the chemical domain of the K-S in the M^{+}-4Si-R^{2+} ternary diagram (Figure 7b). These minerals show slight chemical variations in terms of their Si and Al contents. One population (K-S 1 in Table 2) has high Si (3.45 atoms on the basis of 11 oxygens) and low Al contents (2.24 atoms on the basis of 11 oxygens) and plots in the kaolinite-poor K-S domain. The second population (K-S 2 in Table 2) has less Si (3.18 atoms on the basis of 11 oxygens), greater Al contents (2.69 on the basis of 11 oxygens) and plots in the kaolinite rich K-S domain. Finally, the tubular particles oberved both on the amphibole tooth or on K-S have a halloysite composition (Table 2).

These observations reveal that saponite and montmorillonite are the first clay minerals to crystallize on

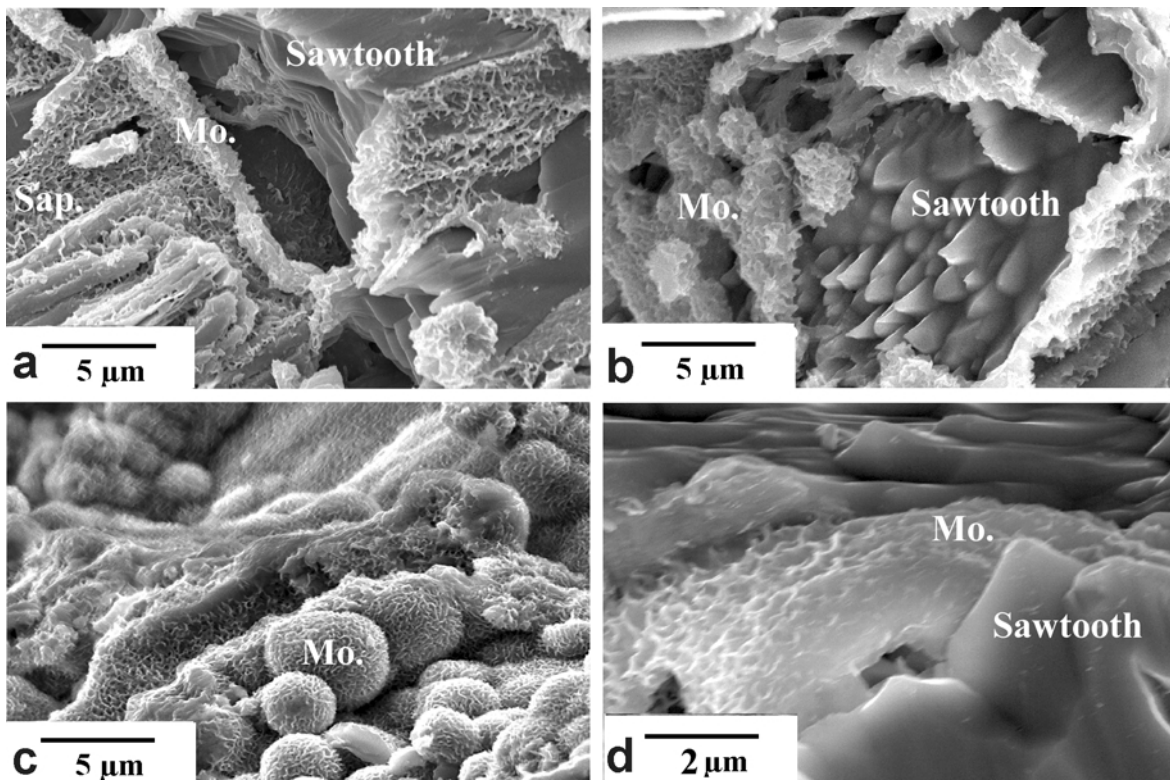

Figure 8. SEM images of early smectite crystallizations in amphibole grains from sample 1: (a) saponite (Sap.) covering the (110) plane and montmorillonite (Mo.) crystallizing in a (001) microcrack; (b) sawtooth termination in a (001) amphibole fracture plane covered with montmorillonite (Mo.); (c) honeycomb spheroidal crystallization of montmorillonite (Mo.) on a (001) amphibole plane; (d) honeycomb layer crystallization of montmorillonite (Mo.) on a sawtooth surface.

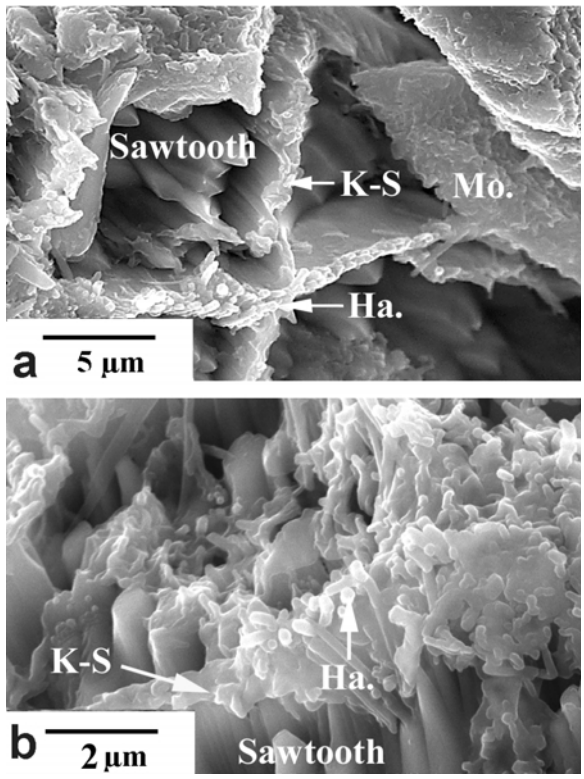

Figure 9. SEM images of a smectite, interstratified K-S and halloysite crystallization sequence on (001) planes of amphibole grains from sample 1: (a) mixed-layer K-S (K-S) and halloysite (Ha.) crystallization at the top of a sawtooth, covered with a montmorillonite (Mo.) honeycomb layer; (b) crystallization of halloysite (Ha.) on mixed-layer K-S (K-S).

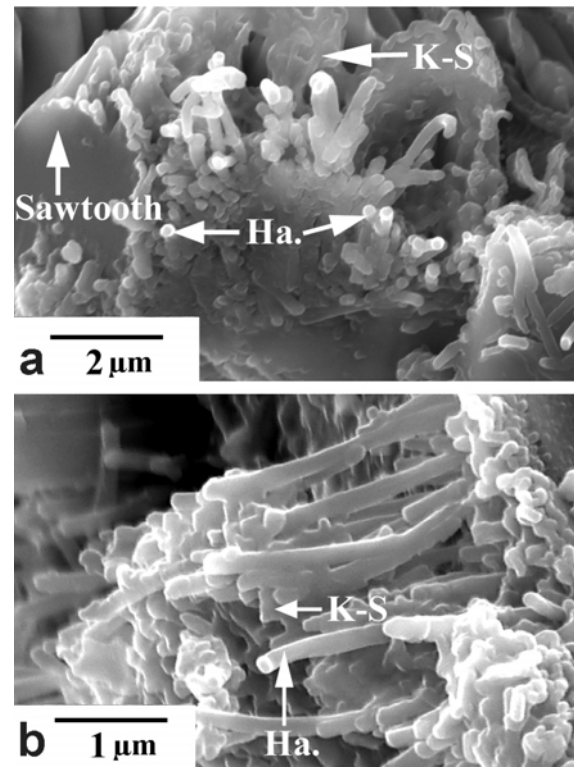

Figure 10. SEM observations of the last stage of the crystallization sequence on a (001) amphibole surface: (a) interstratified K-S (K-S) and halloysite (Ha.) on sawteeth, showing tubular halloysite; (b) tubular halloysite (Ha.) on interstratified platy K-S (K-S).

the (110) and (001) amphibole planes, respectively (Figure 3c, Figure 8a). Saponite appears to be the only clay mineral formed by the amphibole weathering along the (110) surface whereas the weathering clay mineral assemblage on the (001) surface is more complex: the dissolution process on this surface leads to the formation of denticulations and the development of voids between this last surface and the montmorillonite layer (Figure 3d, Figure 8b). Platy particles of K-S (Figure 9a) then appear on the sawtooth. Finally, the later stage of crystallization is characterized by tubular clay particles of halloysite developed either directly on the top of sawtooth or on the platy K-S particles (Figure 9b).Therefore, the following crystallization sequence on the (001) surface can be proposed: montmorillonite → K-S → halloysite.

DISCUSSION

The mineralogical data collected from the weathered amphibole grains in the studied saprolite indicate that four clay mineral species can crystallize in a single amphibole crystal. These newly formed clay minerals appear in a chronological crystallization sequence with no evidence of conversion of one early clay mineral species to another. They mimic a weathering sequence currently observed at the sample scale in the saprolites of ultrabasic and basic rocks, *i.e.* saponite, montmorillonite, mixed-layer K-S and halloysite. This weathering sequence involves a crystallographic and chemical evolution from 2:1 tri- and dioctahedral layer type smectites to 1:1 aluminous layer-type halloysite with intermediate mixed-layer K-S structures. The authors currently relate this crystallographic and chemical evolution to the change from closed (2:1 smectite crystallization) to opened (1:1 kaolinite/halloysite crystallization) weathering systems with increasing chemical leaching (Delvaux *et al.*, 1990; Wakatsuki and Rasyidin, 1992; Watanabe *et al.*, 1992; Jolicoeur *et al.*, 2000; Islam *et al.*, 2002; Wilson, 2004; Price *et al.*, 2005).

In the saprolite studied, the same clay mineral assemblage described above is observed, but at the scale of the amphibole crystal. However, SEM observations allow further study of the weathering processes by assigning each clay mineral species to a specific crystallization microsite. The SEM data reveal that (1) the early formed clay minerals are very specific to given crystallization surfaces, and (2) at the scale of a

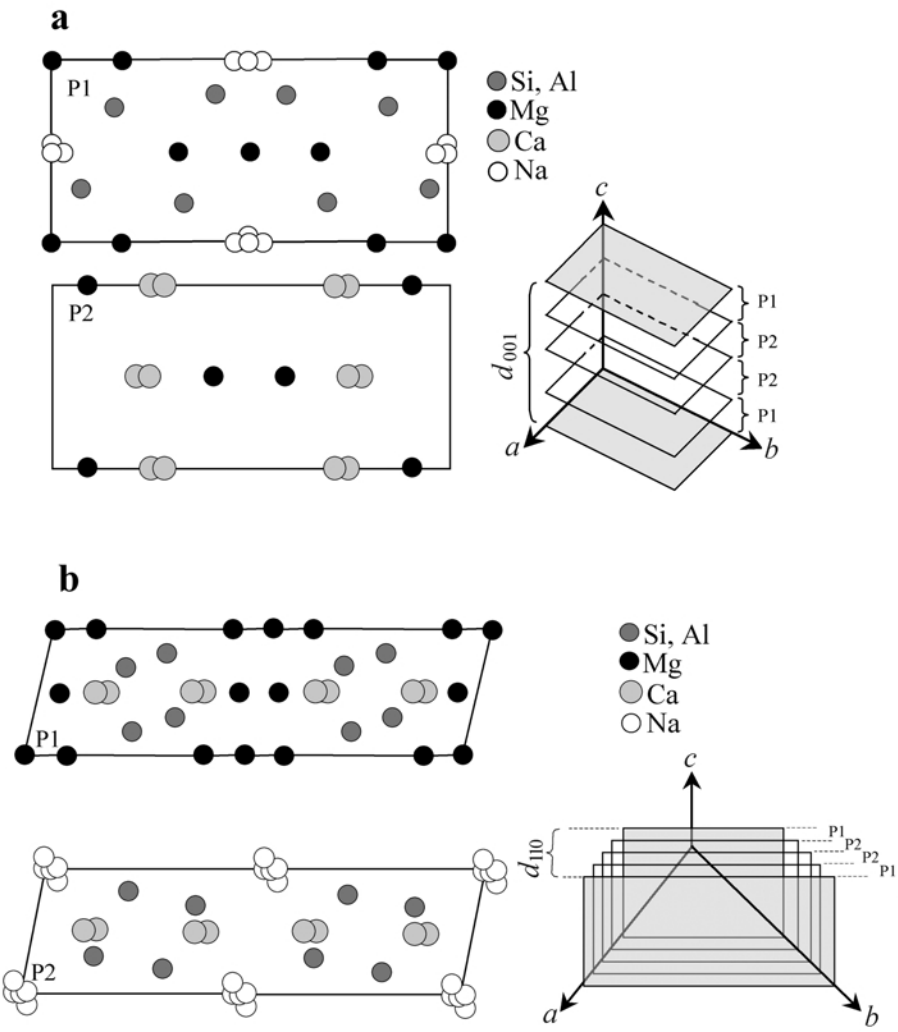

Figure 11. View of atomic distribution in stacked (001) and (110) layers as a function of increasing depth within amphibole. P1 and P2 layers have thickness ranging from 0 to 0.25 d_{hkl} and from 0.25 d_{hkl} to 0.5 d_{hkl}, respectively: (a) view of atomic distribution in stacked P1 and P2 (001) layers; (b) view of atomic distribution in stacked P1 and P2 (110) layers .

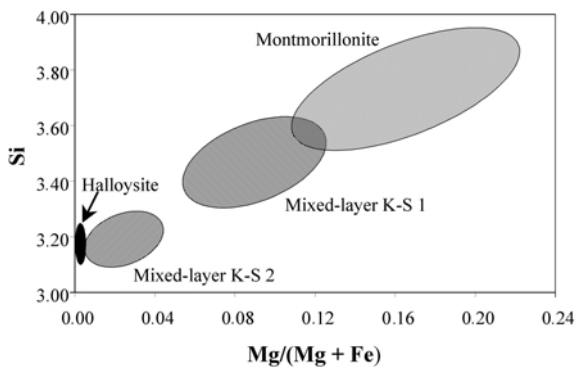

Figure 12. Chemical compositions of clay minerals crystallizing on the (001) amphibole surface plotted in the Si *vs*. Mg/(Mg+Fe) diagram and showing linear evolution from montmorillonite to halloysite. Intermediate compositions refer to mixed-layer K-S 1 with 60% kaolinite component and mixed-layer K-S 2 with 86% kaolinite component.

microsite, on the (001) surface, a complete crystallization sequence of clay minerals can develop with montmorillonite, K-S and halloysite. The differentiation of clay minerals assemblages as a function of the crystallization surfaces within a single amphibole grain can be related either to the differences in surface chemistry and/or the degree of opening of a microsite.

If one considers that the early weathering microsystems operate in closed conditions, the mineralogy of their clay minerals will be strictly controlled by the chemistry of the crystallization surfaces and the dissolution processes which operate on them. To understand the weathering evolution, the nature and arrangement of atoms available on a surface during the dissolution processes can be followed, at the scale of the unit-cell, perpendicular to the (110) and (001) faces at increasing depth in the amphibole crystal (depth interval increment of 0.25 d_{hkl}). The atoms observed

within the first 0.25 d_{hkl} interval (from the surface) are grouped in a single atomic layer (P1 in Figure 11), while the atoms of the next 0.25 d_{hkl} interval constitute the P2 layer in Figure 11. The whole unit-cell can be described by the symmetrical diad effect applied to these two atomic layers.

Thus, in the early weathering stages, the evolution of the nature and arrangement of atoms on the surfaces of the host amphibole unit-cell (P1 layers) show that the (110) surface can release Si, Al and large amounts of Mg (P1 layer in Figure 11a) which promote saponite formation. At the same time, weathering of the (001) surface can release Si, Al but small amounts of Mg (P1 layer in Figure 11b), which does not produce saponite but montmorillonite. In these early weathering steps, it appears that the microsites operate in confined conditions in which the mineralogy of smectites is strictly controlled by the chemistry of the crystallization surfaces.

As weathering proceeds, the dissolution processes operate in two different ways according to the microsites considered. The dissolution which proceeds perpendicular to the (110) surface reaches an atomic layer composed mainly of Si, Al and Ca (P2 layer in Figure 11a). The lack of Mg in this layer seems to slow down or even inhibit the crystallization of saponite or another clay mineral. The dissolution which proceeds perpendicular to the (001) surface reaches the Ca and Mg layer (P2 layer in Figure 11b), which can be leached easily, and allows dissolution to continue. The formation of the sawtooth terminations is favored, leading to the void opening in the microsite. These weathering features constitute circulation paths through which leaching processes are enhanced. Consequently, the weathering microsystems are more and more opened inducing faster leaching and, hence, an important dilution effect on solutions. This chemical evolution influences the mineralogy of the newly formed clay minerals.

This mineralogical evolution on the (001) plane is characterized by successive formation of montmorillonite, mixed-layer K-S 1 and K-S 2, up to halloysite (Figure 12). This mineralogical sequence can be related to the linear decrease in the Mg/(Mg+Fe) ratio and in Si atomic content. The linear behaviour of this evolution indicates that, even if leaching rates of Si and Mg are different, they are constant during the weathering process. Moreover, the decrease in Mg concentration within the solutions with time leads to the clay minerals assemblages becoming richer in the kaolinite component, eventually reaching the pure halloysite end-member. This mineralogical trend is correlated with a strong decrease in the range of chemical composition variations for the different clay minerals. The chemistry of the weathering products gives evidence of the amphibole surface chemistry at a given step of weathering process. This is in contradiction to the possibility of extraneous solutions (coming downwards from higher up in the profile and in equilibrium with bulk saprolite) controlling the formation of the secondary phases. In that case, clay minerals would crystallize anywhere upon all amphibole faces and would not be specific to the observed microsites.

CONCLUSIONS

At the scale of the weathering profile, the clay mineral assemblage resulting from the weathering of the saprolite from Puycheny is mainly composed of dioctahedral smectite (montmorillonite), K-S and halloysite. At the scale of the weathering mineral grain, the clay mineral assemblage is more complex. Depending on the microsites, mineralogy can exhibit a large discrepancy in spatial distribution of clay mineral species. This is particularly true when dealing with amphibole weathering. Thus, dioctahedral smectite appears in the early stages of weathering along the (001) amphibole face, whereas trioctahedral smectite (saponite), not detected in bulk analysis, is the only species which crystallizes along the (110) face.

On the other hand, a specific sequence of clay minerals, montmorillonite, K-S and halloysite, is recognized at the scale of the (001) amphibole face with two stages of K-S crystallization, determined by their kaolinite contents, 60% and 86% respectively. This K-S 1 to K-S 2 evolution step was not recognized in the bulk analysis which gives only an intermediate K-S mineralogical composition. These results indicate that study of basic and ultrabasic saprolites requires knowledge of the relationships between primary magnesian minerals and their weathering products at the scale of microsites. It is thus possible to identify all the clay minerals which play important roles in weathering and could remain undetected in bulk studies due to their small amounts.

REFERENCES

Abreu, M.M. and Vairinho, M. (1990) Amphibole alteration to vermiculite in a weathering profile of gabbro-diorite. Pp. 493–500 in: *Soil Micromorphology* (L.A. Douglas, editor). Developments in Soil Science, **19**. Elsevier, Amsterdam.

Bain, D.C., Roe, M.J., Duthie, D.M.L. and Thomson, C.M. (2001) The influence of mineralogy on weathering rates and processes in an acid-sensitive granitic catchment. *Applied Geochemistry*, **16**, 931–937.

Banfield, J.F. and Barker, W.W. (1994) Direct observation of reactant-product interfaces formed in natural weathering of exsolved, defective amphibole to smectite: Evidence for episodic, isovolumetric reactions involving structural inheritance. *Geochimica et Cosmochimica Acta*, **58**, 1419–1429.

Baronnet, A. (1997) Silicate microstructures at the sub-atomic scale. *Comptes Rendus de l'Académie des Sciences, Série II a: Sciences de la Terre et des Planètes*, **324**, 157–172.

Brantley, S.L. and Chen, Y. (1995) Chemical weathering rates of pyroxenes and amphiboles. Pp. 119–172 in: *Chemical Weathering Rates of Silicate Minerals* (A.F. White and S.L. Brantley, editors). Reviews in Mineralogy, **31**,

Mineralogical Society of America, Washington, D.C.
Caillaud, J., Proust, D., Righi, D. and Martin, F. (2004) Fe-rich clays in a weathering profile developed from serpentinite. *Clays and Clay Minerals*, **52**, 779–791.
Cole, W.F. and Lancucki, C.J. (1976) Montmorillonite pseudomorphs after amphibole from Melbourne, Australia. *Clays and Clay Minerals*, **24**, 79–83.
Delvaux, B., Herbillon, A.J., Vielvoye, L. and Mestdagh, M.M. (1990) Surface properties and clay mineralogy of hydrated halloysitic soil clays. II. Evidence for the presence of halloysite/smectite (H/Sm) mixed-layer clays. *Clay Minerals*, **25**, 141–160.
Dreher, P. and Niederbudde, E.A. (2000) Characterization of expandable layer silicates in humic-ferralic cambisols (umbrept) derived from biotite and hornblende. *Journal of Plant Nutrition and Soil Science*, **163**, 447–453.
Eggleton, R.A. (1975) Nontronite topotaxial after hedenbergite. *American Mineralogist*, **60**, 1063–1068.
Eggleton, R.A. (1982) Weathering of enstatite to talc through a sequence of transitional phases. *Clays and Clay Minerals*, **30**, 11–20.
Eggleton, R.A. and Smith, K.L. (1983) Silicate alteration mechanisms. *Sciences Géologiques, Mémoire*, **71**, 45–53.
Ildefonse, Ph. (1980) Mineral facies developed by weathering of a meta-gabbro, Loire Atlantique (France). *Geoderma*, **24**, 257–273.
Ildefonse, Ph., Copin, E. and Velde, B. (1979) A soil vermiculite formed from a meta-gabbro, Loire-Atlantique, France. *Clay Minerals*, **14**, 201–210.
IMA (1978) Nomenclature of amphiboles. *Mineralogical Magazine*, **42**, 533–563.
Islam, M.R., Peuraniemi, V., Aario, R. and Rojstaczer, S. (2002) Geochemistry and mineralogy of saprolite in Finnish Lapland. *Applied Geochemistry*, **17**, 885–902.
Jolicoeur, S., Ildefonse, Ph. and Bouchard, M. (2000) Kaolinite and gibbsite weathering of biotite within saprolites and soils of Central Virginia. *Soil Science Society of America Journal*, **64**, 1118–1129.
Kampf, N., Schneider, P. and Mello, P.F. (1995) Alteracoes mineralogicas em sequencia vertissolo-litossolo na Regiao da Campanha no Rio Grande do Sul. *Revista Brasileira de Ciencia do Solo*, **19**, 349–357.
Lanson, B. (1993) *DECOMPXR, X-ray Decomposition Program*. ERM, Poitiers, France.
Luce, R.W., Bartlett, R.W. and Parks, G.A. (1972) Dissolution kinetics of magnesium silicates. *Geochimica et Cosmochimica Acta*, **36**, 35–50.
Price, J.R., Velbel, M.A. and Patino, L.C. (2005) Rates and time scales of clay-mineral formation by weathering in saprolitic regoliths of the southern Appalachians from geochemical mass balance. *Geological Society of America Bulletin*, **117**, 783–794.
Proust, D. (1982) Supergene alteration of hornblende in an amphibolite from Massif Central (France). Pp. 357–364 in: *Proceedings of the 7th International Clay Conference, Bologna-Pavia*, 1981 (H. van Olphen and F. Veniale, editors). Developments in Sedimentology, **35**, Elsevier, Amsterdam.
Proust, D. (1985) Amphibole weathering in a glaucophane-schist (Ile de Groix, Morbihan, France). *Clay Minerals*, **20**, 161–170.
Proust, D. and Velde, B. (1978) Beidellite crystallization from plagioclase and amphibole precursors: local and long-range equilibrium during weathering. *Clay Minerals*, **13**, 199–209.
Reynolds, R.C. (1985) *NEWMOD, a computer program for the calculation of one-dimensional diffraction powders of mixed-layer clays*. R.C. Reynolds, 8 Brook Rd., Hanover, New Hampshire 03755 USA, 315 pp.
Righi, D. and Meunier, A. (1995) Origin of clays by rock weathering and soil formation. Pp. 43–161 in: *Origin and Mineralogy of Clays. Clays and the Environment* (B. Velde, editor). Springer-Verlag, Berlin.
Righi, D., Terribile, F. and Petit, S. (1998) Pedogenic formation of high-charge beidellite in a vertisol from Sardinia (Italy). *Clays and Clay Minerals*, **46**, 167–177.
Righi, D., Terribile, F. and Petit, S. (1999) Pedogenic formation of kaolinite-smectite mixed layers in a soil toposequence developed from basaltic parent material in Sardinia (Italy). *Clays and Clay Minerals*, **47**, 505–514.
Schott, J., Berner, R.A. and Sjöberg, E.L. (1981) Mechanism of pyroxene and amphibole weathering. I. Experimental studies of iron-free minerals. *Geochimica et Cosmochimica Acta*, **45**, 2123–2135.
Velbel, M.A. (1989) Weathering of hornblende to ferruginous products by a dissolution-reprecipitation mechanism: petrography and stoichiometry. *Clays and Clay Minerals*, **37**, 515–524.
Wakatsuki, T. and Rasyidin, A. (1992) Rates of weathering and soil formation. *Geoderma*, **52**, 251–263.
Watanabe, T., Sawada, Y., Russell, J.D., McHardy, W.J. and Wilson, M.J. (1992) The conversion of montmorillonite to interstratified halloysite-smectite by weathering in the Omi acid clay deposit, Japan. *Clay Minerals*, **27**, 159–173.
Wegner, M.W. and Christie, J.M. (1985) Chemical etching of amphiboles and pyroxenes. *Physics and Chemistry of Minerals*, **12**, 86–89.
Wilson, M.J. (1987) Soil smectites and related interstratified minerals: Recent developments. Pp. 167–173 in: *Proceedings of the International Clay Conference, Denver, 1985* (L.G. Schultz, H. van Olphen and F. A. Mumpton, editors). The Clay Minerals Society, Bloomington, Indiana.
Wilson, M.J. (2004) Weathering of the primary rock-forming minerals: processes, products and rates. *Clay Minerals*, **39**, 233–266.
Wilson, M.J. and Farmer, V.C. (1970) A study of weathering in a soil derived from a biotite-hornblende rock. II. The weathering of hornblende. *Clay Minerals*, **8**, 435–444.
Zhang, H. and Bloom, P.R. (1999a) The pH dependence of hornblende dissolution. *Soil Science*, **164**, 624–632.
Zhang, H. and Bloom, P.R. (1999b) Dissolution kinetics of hornblende in organic acid solutions. *Soil Science Society of America Journal*, **63**, 815–822.
Zhang, H., Bloom, P.R., Nater, E.A. and Erich, M.S. (1996) Rates and stoichiometry of hornblende dissolution over 115 days of laboratory weathering at pH 3.6–4.0 and 25ºC in 0.01 M lithium acetate. *Geochimica et Cosmochimica Acta*, **60**, 941–950.

(*Received 23 September 2005; revised 7 December 2005; Ms. 1093*)